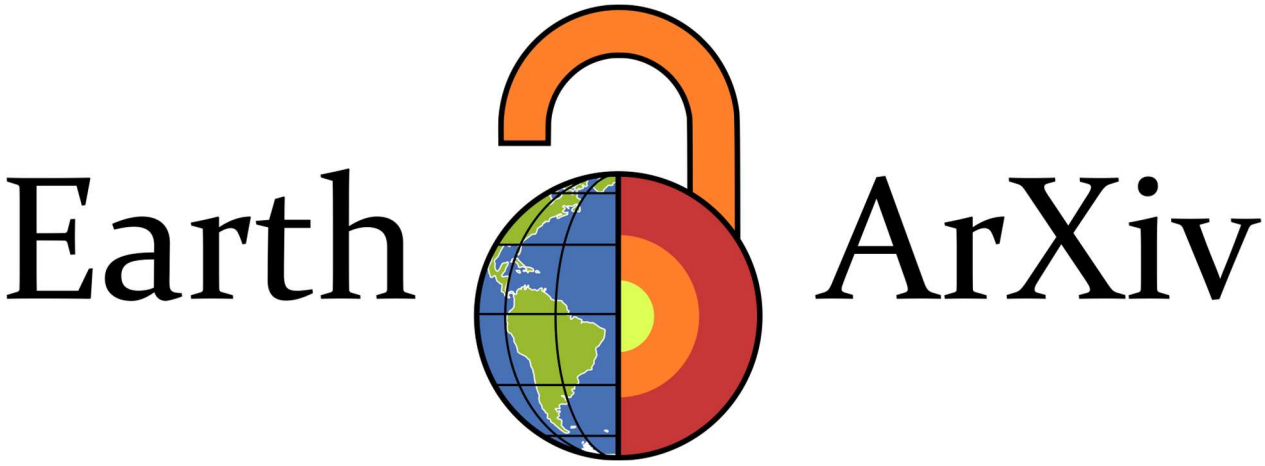

Bayesian Estimation of Paleoearthquake Magnitudes in the Central Apennines

Deborah Di Naccio[1*], Davide Zaccagnino[1,2,*], Michele Matteo Cosimo Carafa[1]

[1] National Institute of Geophysics and Volcanology (INGV), Via di Vigna Murata 605, 00143 Rome, Italy

[2] Institute of Risk Analysis, Prediction and Management (Risks-X), Academy for Interdisciplinary Studies, Southern University of Science and Technology (SUSTech); 1088 Xueyuan Rd., Shenzhen, Guangdong, China, 518055

*corresponding author: davidezaccagnino@gmail.com

Michele Carafa: michele.carafa@ingv.it

Davide Zaccagnino: zaccagnino@sustech.edu.cn

Deborah Di Naccio: https://orcid.org/0000-0002-0344-1173

Davide Zaccagnino: https://orcid.org/0000-0001-6884-8452

Michele Matteo Cosimo Carafa: https://orcid.org/0000-0001-5463-463X

Key Points

1. New database of paleoseismic events in the central Apennines (PaleoECA_2025)
2. New Bayesian inversion algorithm with joint slip, length and age data (PaleoBayes)
3. Uncertainties must be carefully considered when applying paleoseismic magnitude estimations to seismic hazard

Abstract

Paleoseismic data provide critical constraints on earthquake recurrence where instrumental records are limited, but magnitude estimation from geologic evidence requires careful treatment of measurement uncertainties. We develop a Bayesian method with application to

the estimation of paleoearthquake magnitudes in the central Apennines, Italy, by jointly analyzing rupture length (L), slip (S), and age (T) data from field investigations. Our framework incorporates empirical scaling relationships with their full uncertainty time-dependent preservation probabilities, and physically informed priors. After the calibration of the best model, our analysis returns magnitude estimates that show agreement with existing parametric catalogs for some historical and instrumental earthquakes while revealing systematic differences with other key events. For the 1915 Fucino earthquake, our result (Mw 6.76±0.07) suggests slight overestimation in past research (Mw ~ 6.8-7.1). The method demonstrates stable performance across 44 paleoevents reported in a new, freshly released database (PaleoECA_2025), with credible intervals mostly in the range ± (0.1-0.3) reflecting measurement uncertainties and preservation bias. We observe that results depend critically on the chosen scaling laws (tested against, e.g., Wells and Coppersmith 1994, Leonard 2010). This approach provides a reproducible framework, also publicly available in the MATLAB software (PaleoBAYES), for quantifying uncertainties in paleoseismic databases. Discrepancies with some historical estimates highlight the importance of systematic, uncertainty-aware methods when deriving magnitudes from paleoseismological data.

Introduction

One of the main challenges in paleoseismology is constraining the age and offset of past earthquakes to estimate their magnitudes and the earthquake history of active faults. The coseismic offset and rupture length provide clues about the earthquake's magnitude (e.g., Wells and Coppersmith, 1994; Leonard, 2014). This is especially important for silent faults where no instrumental or historical records are available. However, this process requires caution. Several

48 factors, such as secondary coseismic effects or subsequent exogenous phenomena are often
49 difficult to distinguish from primary faulting. This may cause local exaggerated fault exposure or
50 obliteration of its plain (Di Naccio et al., 2019; Kastelic et al., 2017). Furthermore, data sampling
51 is not random but depends on preserving features, offset size, and accessibility issues. Larger
52 offsets are more likely to be preserved and may be over-represented. To ensure robust estimates,
53 rigorous statistical methods are required (Carafa et al., 2022; Bird, 2007). The variability along the
54 strike of earthquake ruptures further complicates the use of single-site data to represent the entire
55 event. Therefore, it is essential to develop methods that can account for this variability. For
56 instance, Brozzetti et al. (2019) found that the rupture parameters for the 24 August 2016
57 earthquake in central Italy are well within the values predicted by the empirical regressions.
58 However, for the 30 October 2016 event, the maximum and average displacements (D_{max} and D_{avg})
59 divert significantly, with D_{max} much higher and D_{avg} significantly lower than the expected values
60 from commonly used regression relationships (Wells and Coppersmith, 1994; Pavlides and
61 Caputo, 2004). On the other hand, the Surface Rupture Length (SRL) approaches the empirical
62 regressions better than D_{max} and D_{avg}. These aspects raise questions about the reliability of the
63 regressions between magnitude and displacement, as the data used for constructing these equations
64 may have similar issues. It has also been proven that the simultaneous use of independent
65 measurements (length of surface rupture and displacement) reduces the estimated earthquake
66 magnitudes and the associated uncertainty (Biasi and Weldon, 2006; Styron and Sherrod, 2021).

67 This study aims to enhance the accuracy of estimating the magnitudes of past earthquakes using
68 field geological data and advanced statistical methods. We explore the probability that an
69 earthquake of magnitude Mw produces a surface displacement D along a fault with rupture length
70 L. Empirical relationships exist linking magnitude with both displacement and fault length, and

these relationships form the basis of our analysis. In the context of paleoseismological data in the Central Apennines, this region experiences the largest and most frequent earthquakes in the entire chain (Rovida et al., 2020; 2022). This characteristic has favored neotectonic studies, resulting in a substantial amount of paleoseismological data, i.e., displacement D, along with their associated uncertainties and a corresponding range for coseismic rupture length L, also with its uncertainties. This aspect is fundamental for understanding the relation between the energy released by an earthquake and the surface deformations. Assuming a tapered Gutenberg-Richter distribution for the regional seismicity, we want to explore the probability of observing a displacement D and define in this way a threshold magnitude as a pseudo-completeness of the paleoseismological catalog.

The target area extends over 100 km along the extensional domain of the central Apennines, from the Campo Imperatore basin to the Aremogna-Cinque Miglia plain. We accomplish a Bayesian estimation of the magnitudes of paleo earthquakes that occurred in Central Italy during the last ~25k years by combining multiple measurements onsite of the rupture length, displacement, and event age. This is based on a priori information, p(M), geological and structural constraints, and involves the simultaneous use of linear regression laws for rupture length and displacement. In this way, the rupture length and average displacement values are sampled by its own Probability Density Function, (p(L|M) and p(D|M)), describing its variability.

Studied area and seismotectonic background.

The central Apennines is one of the most seismically active regions in peninsular Italy. In recent times, several Mw+ 6.0 earthquake sequences have occurred, including the April 6, 2009 (Mw 6.1) event and the August-October 2016 sequence (Mw 6.0-6.5) (ISIDe Working Group, 2007; Latorre et al., 2022). Historical records also document devasting earthquakes, such as those on January 13,

1915 (Mw 7.1), February 2, 1703 (Mw 6.7), September 9, 1349 (Mw 6.8), November 27, 1461 (Mw 6.5), and July 24, 1654 (Mw 6.3) (Rovida et al., 2020; 2022). Towards the Adriatic side, seismic activity is moderate. However, regional analyses, including those by Carafa and Bird (2016), suggest that the deformation in this area is extensional and accompanied by minor seismicity, which may include the Majella event on November 3, 1706 (MW 6.8). Additionally, trenching studies have provided evidence of surface coseismic ruptures from the Late Pleistocene-Holocene period (Galli et al., 2008; Galli, 2020; Cinti et al., 2021; Lombardi et al., 2025).

Geological, geodetic, and seismological data consistently indicate an active SW-NE tensional stress field with an estimated deformation rate ranging from 2.5 to 3.5 mm/year for the extension between the Tyrrhenian and Adriatic coasts (e.g., Carafa and Bird; 2016, Devoti et al., 2017; Carafa et al., 2020, Mariucci and Montone, 2024; Carafa and Barba, 2013; Pondrelli and Salimbeni, 2006). The active Pleistocene-Holocene extension began in the hinterland domain of the Apennines (Tyrrhenian side) and has since migrated eastward (Lavecchia et al., 1994; Carminati and Doglioni, 2012; Montone and Mariucci, 2016; Pondrelli and Morelli, 2008). This extension currently affects a narrow belt approximately 80 km wide that cuts through and is superimposed on post-Miocene thrusts and folds within the accretionary wedge (Patacca et al., 2008).

The extension of the Apennine crust is accommodated by seismogenic faulting in its brittle portion. The brittle-ductile transition (BDT) is located at depths greater than 12 to 16 km and becomes thicker towards the south and east as indicated by seismological studies and catalogs (Frepoli et al., 2017; Valoroso et al., 2013; Latorre et al., 2023; Chiarabba et al., 2005). In the past decades, several compilations of Pleistocene–Holocene active faults have been published (Galadini and Galli, 2000; Carafa et al., 2022; Lavecchia et al., 2022; Faure Walker et al., 2021), primarily

117 relying on long-term geomorphic expression, such as half-graben intramountain basins (e.g.,
118 Fucino and Sulmona basins), dislocated Late Pleistocene (<126 kyr)-Holocene breccias, or
119 cumulated offset since the Last Glacial Maximum. The fault systems, striking from NW-SE to
120 NNW-SSE, consist of high-angle normal and normal-oblique faults (Galadini and Galli, 2000;
121 Lavecchia et al., 2022; Carafa et al., 2020) as well as inherited structures (Pizzi and Galadini, 2009;
122 Di Domenica et al., 2012; Porreca et al., 2020) that mainly dip towards SW. A visual representation
123 of the investigated region is provided in **Figure 1**.

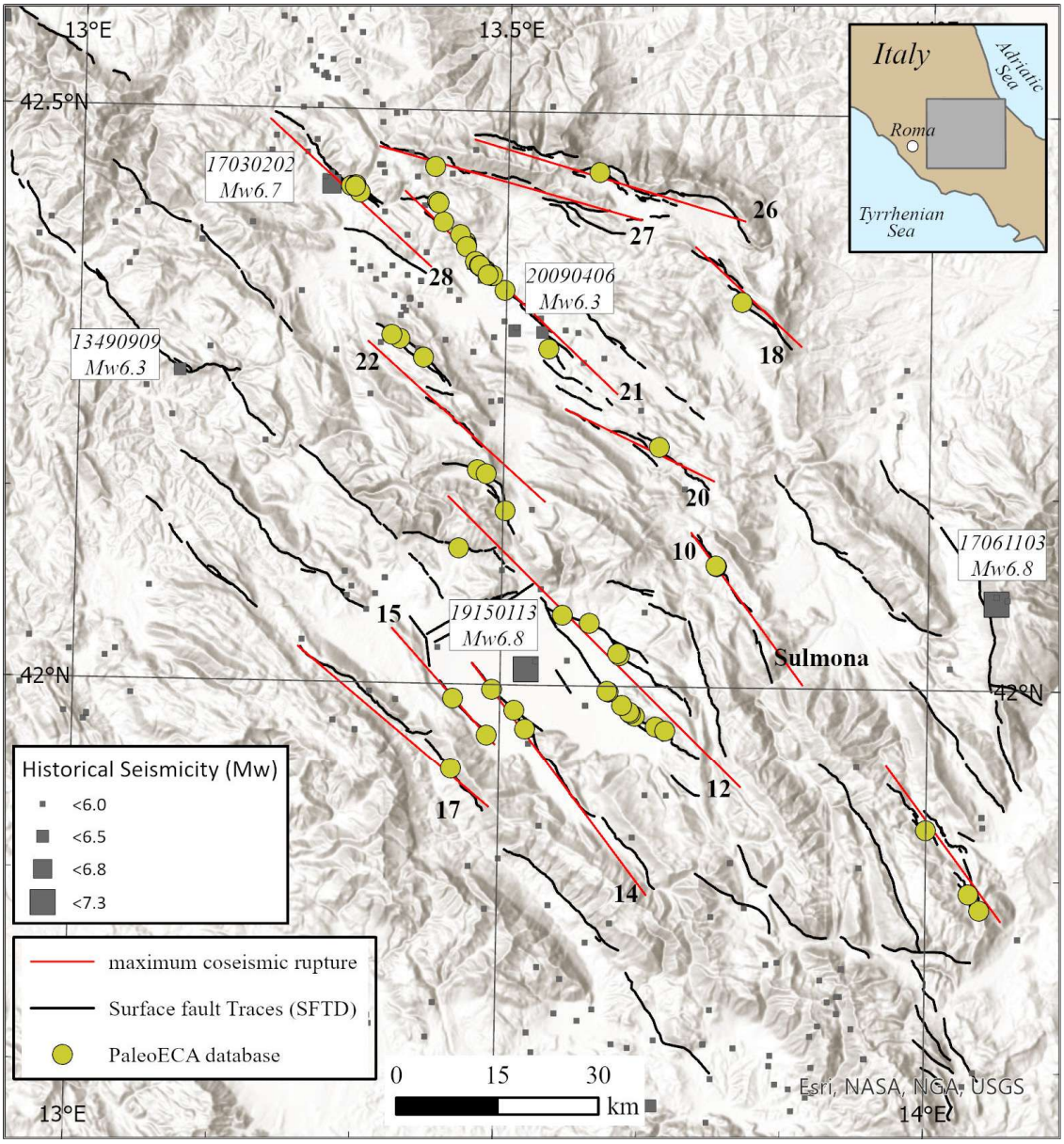

Figure 1: Map of the study area showing the measurement points of paleoearthquakes in the central Apennines (PaleoECA_2025 database), the surface-active fault traces (SFTD), and the maximum coseismic rupture length derived by the Fault Sources Database, (FSD) available in Di Naccio et al., 2025.

Geological model - input data

We collected coseismic deformation data through a comprehensive review of paleoseismological and historical records dating back to 1986 (Serva et al., 1986). We excluded data where the offset measurements were reported as cumulative displacement or slip per event, as these values often represent an average over multiple ruptures rather than a single event.

The resulting database contains 125 records of individual earthquakes that occurred in central Italy over the last ~25k years. Each record includes information on the event age, displacement, rupture length, and associated uncertainties with data gathered from 52 measurement sites along 13 active faults (Carafa et al., 2020; 2022; Di Naccio et al., 2025).

For each of these 13 active faults, we identified 44 individual earthquake events (En), labeling them from the most recent (E1, representing the last earthquake) to the oldest one (E7, the maximum number of events recorded for a given fault). Correlations between events within a fault system were established only when explicitly stated by the authors, to avoid subjective interpretation. This cautious approach was adopted despite the availability of several statistical methods developed in recent times (Ramsey, 2009). These methods either analyze pairs of overlapping probability curve distributions (DuRoss et al., 2011) or explore multiple correlation scenarios based on the ranges of event ages (Cinti et al., 2021). In both approaches, the likelihood of event correlation remains heavily dependent on expert judgment. To mitigate subjectivity, a recent method has been introduced that accounts for all contributing probability density functions (PDFs), yielding a mean distribution that serves as the final PDF for that event (Gòmez-Novell et al., 2023).

Defining rupture length presents its own challenges. Fault scarps often reflect the cumulative effect of multiple earthquakes, making it difficult to isolate the contribution of individual events.

Additionally, exogenic processes, as well as the influence of highly urbanized and vegetated environments, can impact the preservation of these features. For our analysis, we adopted the fault model developed by Carafa et al. (2022) and Di Naccio et al. (2025) for central Italy. We assume that the maximum rupture length corresponds to the entire extent of the seismogenic fault. The minimum rupture length was estimated by measuring the distance between points where the En earthquake is observed or by analyzing clear ruptures in topography data.

Then, using a probabilistic approach, we estimate the PDF distribution for the offset and rupture length associated with a new database of 44 paleoearthquakes: indeed, a comprehensive database of past earthquakes derived from paleoseismological data is crucial for advancing our knowledge of ongoing tectonic processes, earthquake sources, and seismic behavior, especially where seismic catalogs are limited. Nonetheless, in studying complex geological processes, it is necessary to use a solid probabilistic approach that rigorously explores the uncertainties of the model components, such as throw and age reported in the paleoseismological investigations. Specifically, we accomplish a Bayesian estimation of magnitudes of paleo-events that occurred in central Italy during the last ~25k years by combining multiple measurements onsite of the rupture length, throw, and event age.

Methods

We estimate paleoearthquake magnitudes (M) from field observations of rupture length (L), average slip (S), and time elapsed since occurrence (T) using a Bayesian framework. A visual summary of our algorithm is provided in **Figure 2**.

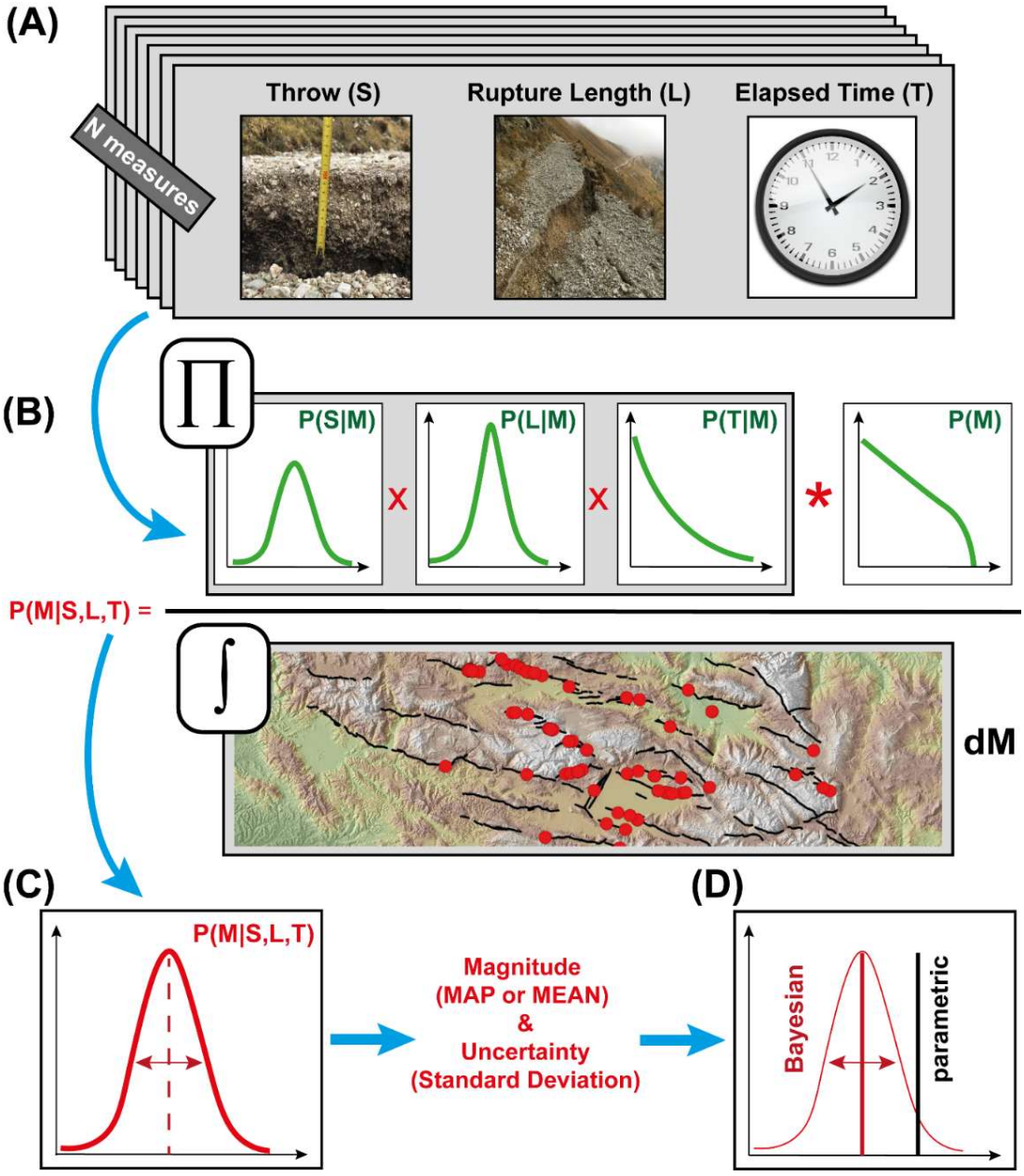

172

173 **Figure 2: Visual summary of the PaleoBAYES algorithm for the estimation of**
174 **paleomagnitudes given the values of the observed rupture length (L), slip (S), and age (T)**
175 **from field investigations.**

176

The approach begins with Bayes' theorem, which updates prior beliefs about M with new data to derive a posterior probability distribution. For n measurements of a single event in paleoseismic trenches, the theorem expresses the posterior $P(M|L_i, S_i, T_i)$ as proportional to the product of the likelihood of observing the data given M and the prior probability of M. To derive this rigorously, we start with the joint probability of all measurements:

$$\mathrm{P}(M, \{L_i, S_i, T_i\}_{i=1}^{n}) = \mathrm{P}(\{L_i, S_i, T_i\}_{i=1}^{n} \mid M)\mathrm{P}(M) \quad (1)$$

where $P(M)$ represents prior knowledge (e.g., Gutenberg-Richter distribution or uniform for large earthquakes). Assuming conditional independence between measurements - meaning L_i, S_i, and T_i for a given M are independent - the likelihood factorizes into

$$P(\{L_i, S_i, T_i\}_{i=1}^{n} \mid M) = \prod_{i=1}^{n} P(L_i, S_i, T_i \mid M). \quad (2)$$

We further decompose $P(L_i, S_i, T_i|M)$ by separating the time-dependent probability that an event be detected in paleoseismic trenches after a time T_i from the physical scaling laws $(L_i, S_i|M)$:

$$P(L_i, S_i, T_i \mid M) = P(L_i \mid M)P(S_i \mid M)P(T_i \mid M). \quad (3)$$

Here, $P(T_i|M)$ simplifies to $P(T_i) = e^{-\lambda T_i}$, as we assume that the probability of detection for large events is dominated by time rather than magnitude. λ is a suitable constant depending on historical and paleoseismic recordings quality, erosion and environmental characteristics supporting offset preservations over time (see a detailed explanation at the end of this paragraph). Combining these steps, the unnormalized posterior becomes

$$P(M \mid \{L_i, S_i, T_i\}_{i=1}^{n}) = P(M) \prod_{i=1}^{n} \left[P(L_i \mid M)P(S_i \mid M)\, e^{-\lambda T_i}\right]. \quad (4)$$

The normalized posterior divides this by the marginal likelihood (the integral of P over M), ensuring probabilities sum to unity:

198 $$P(M \mid \{L_i, S_i, T_i\}_{i=1}^{n}) = \frac{[\prod_{i=1}^{n} P(L_i|M) P(S_i|M) e^{-\lambda T_i}] P(M)}{\int [\prod_{i=1}^{n} P(L_i|M) P(S_i|M) e^{-\lambda T_i}] P(M)\, dM}. \quad (5)$$

199 The likelihood terms $P(L_i|M)$ and $P(S_i|M)$ are modeled as log-normal distributions based on
200 empirical scaling laws:

201 $$\begin{cases} \log L_i = a_L + b_L M + \epsilon L, & \epsilon L \sim N(0, \sigma_L), \\ \log S_i = a_S + b_S M + \epsilon S, & \epsilon S \sim N(0, \sigma_S), \end{cases} \quad (6)$$

202 where a_L, b_L, a_S, b_S are regression coefficients. σ_L, σ_S quantify observational uncertainty and also
203 consider quadratically, via error propagation, single field measurement. $N(0, \sigma)$ represents the
204 normal distribution with zero mean and sigma as standard deviation. Coefficients are retrieved
205 from Wells and Coppersmith (1994) for normal fault types, from Pavlides and Caputo (2004),
206 Leonard (2010) for continental regions with dip slip faulting and Thingbaijam et al. (2017) for
207 further physics-based constraints.

208 Explicitly, the likelihoods are

209 $$P(L_i|M) = \frac{1}{\sqrt{2\pi\sigma_L^2}} \exp\left(-\frac{(\log L_i - a_L - b_L M)^2}{2\sigma_L^2}\right) \quad (7)$$

210 $$P(S_i|M) = \frac{1}{\sqrt{2\pi\sigma_S^2}} \exp\left(-\frac{(\log S_i - a_S - b_S M)^2}{2\sigma_S^2}\right), \quad (8)$$

211 representing the conditional probability density function (PDF) of L and S given M. Note that we
212 expect they are log-normal distributed when conditioned on M. We check the reliability of this
213 assumption by assessing the performance of the log-normal distribution in fitting the empirical
214 cumulative distribution function of throws (S) using the Kolmogorov-Smirnov test for three recent
215 available coseismic datasets with measurements collected just after the occurrence of the Paganica
216 Mw 6.3 2009, Amatrice Mw 6.2 2016 and Norcia Mw 6.6 2016 earthquakes. The Log-Normal

distribution performs satisfactorily in competition with the Gamma and Weibull functions and clearly better than exponentials and power laws. Results are shown in **Figure 3**.

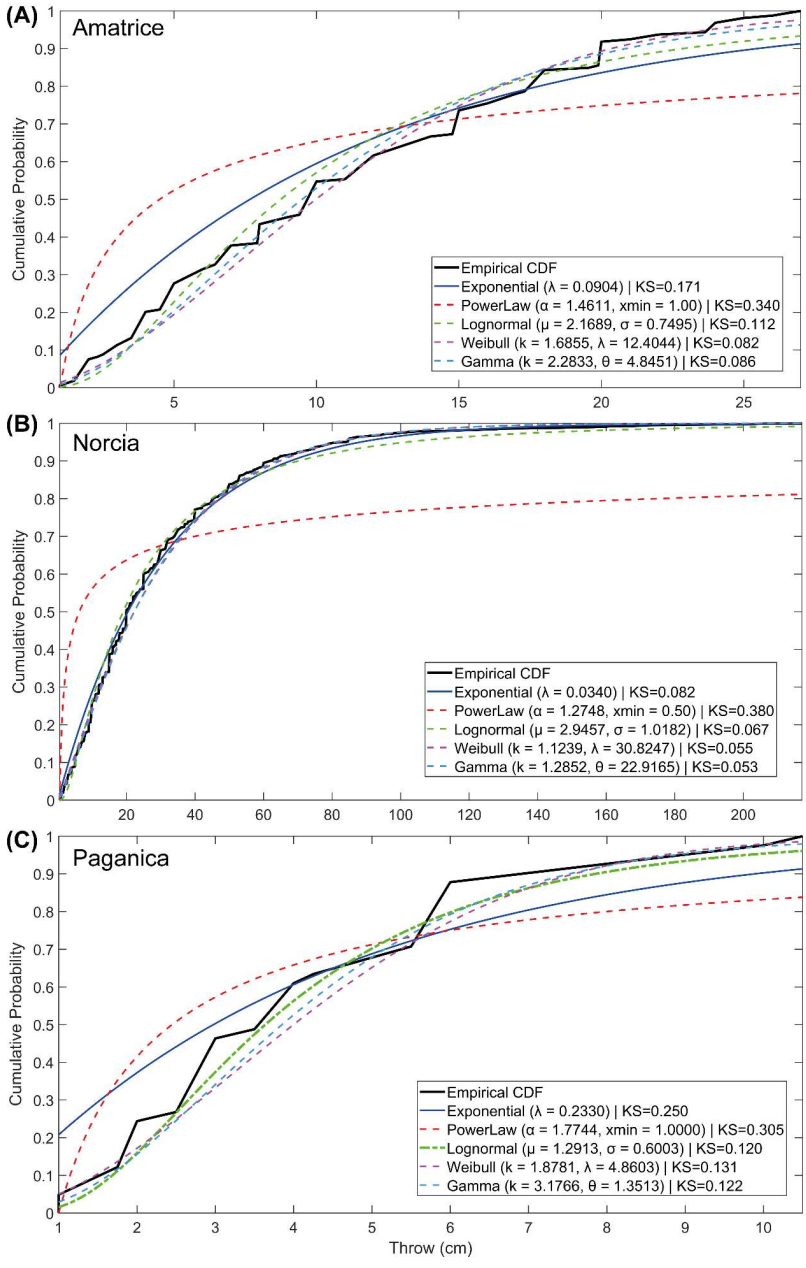

Figure 3: Cumulative probability distributions of throws in the Amatrice (A), Norcia (B) and Paganica (C) region. The output of the Kolmogorov-Smirnov test (KS) for the fit procedure

realized using 5 different distributions shows that the Weibull, Gamma and Log-Normal functions can grasp well the trend of data (from Brozzetti et al., 2019; Nurminen et al., 2022).

The posterior is evaluated numerically by discretizing M into a grid (in our case on the central Apennines, from 5.0 to 7.5 in 0.01 increments). For each M_j, the un-normalized posterior $P(M_j)$ combines the prior, likelihoods, and preservation weights across all measurements. The normalized posterior provides a probability density function of the paleoseismic magnitude. It is typically unimodal, often almost Gaussian when likelihoods dominate the prior function. Its peak defines the maximum *a posteriori* (MAP) estimate, while the 95% credible interval quantifies uncertainty thorough the approximate amplitude in magnitudes of the distribution. Wider intervals arise from sparse data, conflicting measurements, or older ages (T_i), as ancient evidence is downweighed by $e^{-\lambda T_i}$, where $\lambda = 0.1$ (likelihood set such that only in exceptional conditions a paleoearthquake can be identified if occurred more than 30-40k years ago) and the time is expressed in thousand years before present. This approach inherently balances empirical scaling laws, temporal preservation bias, and observational uncertainty to deliver probabilistic magnitude estimates.

Best model selection

As a last step, we need to identify the best model combination for the scaling laws utilized in the Bayesian algorithm among the Wells & Coppersmith (1994), Pavlides & Caputo (2004), Leonard (2010) and Thingbaijam & al. (2017), and the *a priori* distribution of large event magnitudes (uniform or Gutenberg-Richter law). To do it, we introduce the cost function

$$C(M, \sigma;\ M_P) = \sum_{i=1}^{N} \frac{(M_i - M_{Pi})^2}{{\sigma_i}^2} \quad (9)$$

which provides a measure of the ability of each combination of scaling laws to enhance the performance of our algorithm in reproducing a set of magnitudes (M_i) for known seismic events (M_{Pi}) given their uncertainties (σ_i). The lower the output of the cost function, the better the model. In our case, we identify the best model on its performance in reproducing a set of 4 known magnitudes for which independent parametric and seismological measurements are available, i.e., Fucino Mw 6.9 1915, Paganica Mw 6.3 2009, Amatrice Mw 6.2 2016 and Norcia Mw 6.6 2016 earthquakes (Valensise and Pantosti, 2001; Rovida et al., 2022). A visual representation in the case of the Fucino 1915 earthquake is reported in **Figure 4**.

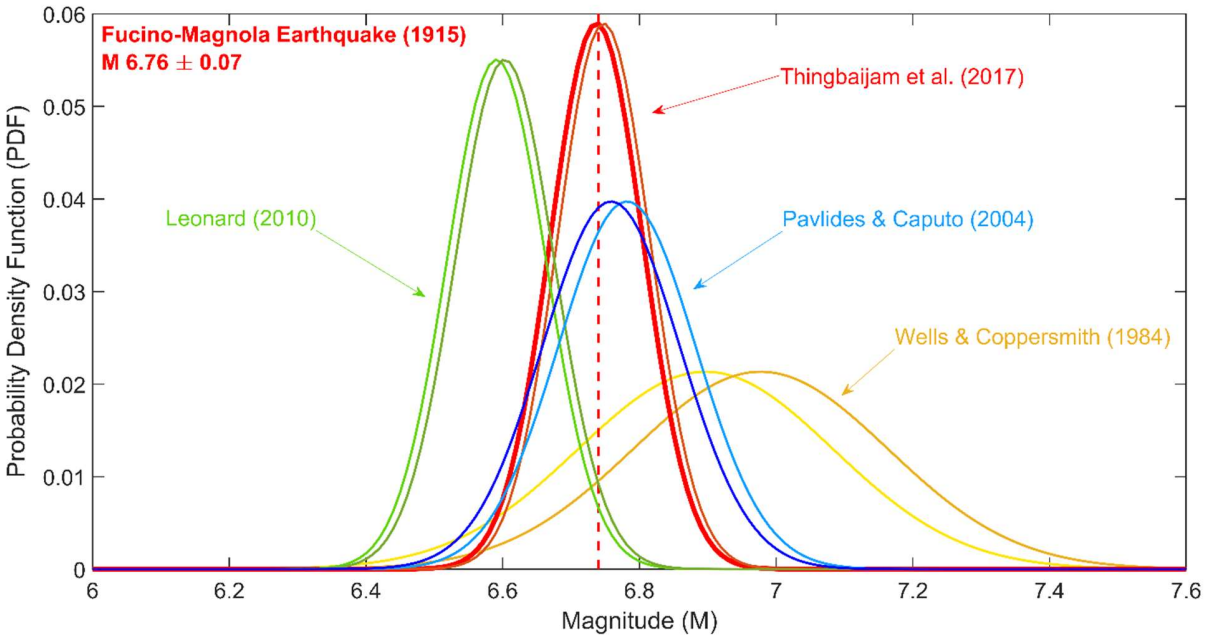

Figure 4: Estimation of the magnitude of the 1915 Fucino earthquake using different scaling laws for rupture lengths and throws (Wells and Coppersmith (1994) in yellow/orange, Pavlides and Caputo (2004) in marine/blue, Leonard (2010) in aquamarine/green and Thingbaijam and al. (2017) in red/bordeaux) and large magnitude distributions (uniform -

right curves - vs Gutenberg-Richter law on the left for each couple). The best model, magnitude and associated uncertainty are highlighted in red and by the vertical dashed line.

Based on the output of this procedure, henceforth in the manuscript we assess paleomagnitudes using the scaling laws for normal faulting earthquakes reported in Thingbaijam et al. (2017) assuming large magnitudes be distributed according to the Gutenberg-Richter law.

Results and Discussions

In this study, we compiled a dataset of 44 paleo- and historical earthquakes and derived their magnitude probability density functions (PDFs) using the methodology outlined earlier. The resulting PDFs (Figures 5–7, Table 1) are generally symmetrical, though not perfectly so, and exhibit magnitude uncertainties ranging between 0.1 and 0.3. While these uncertainties may appear substantial, they are reasonable given the multiple sources of error incorporated into our analysis, including measurement uncertainties in fault throw and rupture length, variability in scaling laws, epistemic uncertainty in fault property scaling relationships, and the choice of prior magnitude-frequency distribution.

Our magnitude estimates obtained using the scaling relationships of Thingbaijam et al. (2017) and assuming a Gutenberg-Richter distribution for large Apennine earthquakes with b-value = 1.0, show broad consistency with parametric magnitude estimations, generally agreeing within 2σ error bounds. For instance, our estimate for the 1915 Fucino earthquake (Mw 6.76 ± 0.07) seems to be consistent with recent reassessments (Mw 6.7, Paolucci et al., 2016) rather than earlier, higher estimates (up to Mw 7.1, Rovida et al., 2020; 2022). However, some results deviate from expectations - most notably, our estimate for the 2009 L'Aquila (Paganica) earthquake (Mw 5.96 ± 0.05) is significantly lower than the widely accepted Mw 6.2-6.3 inferred from seismological analyses (e.g., Walters et al., 2009). This discrepancy may stem from the limited number of coseismic surface ruptures measured, which, when combined with the event's recent occurrence, could introduce a downward bias in magnitude estimation.

In the case of the Paganica Mw 6.3 2009 event, the surface expression of faulting was notably heterogeneous, ranging from warping and open fissures without measurable slip to distributed offset along synthetic splays (Boncio et al., 2010; EMERGEO working group, 2010). Such deformation patterns, often indicative of shallow or incomplete slip propagation, are particularly difficult to interpret. Consequently, the surface geological signal may not reliably capture the full extent of coseismic slip, leading to an underestimation of the earthquake magnitude. Moreover, areas with evidence of surface rupture may have gone unsampled, either due to accessibility issues or environmental conditions, such as dense vegetation, that hindered systematic mapping and introduced spatial sampling bias. These limitations became even more impactful when dealing with paleoearthquakes. In many cases, the occurrence of multiple surface-rupturing earthquakes, postseismic erosion, and the development of angular unconformities obscure the identification of horizontal events, the estimation of coseismic offset, and the reconstruction of a complete paleoseismic history. This issue becomes increasingly evident and impactful for more ancient events, as exogenous processes have had more time to erase geological evidence of past ruptures. This is the reason why we address this temporal bias accounting for time-dependent preservation in our inversion.

While recent earthquakes can be studied through target geological surveys that allow reasonably constrained estimation of surface rupture lengths, despite the logistical and environmental challenges, this approach becomes significantly less reliable for paleo-earthquakes. Empirical regressions based on surface rupture length tend to provide more reliable magnitude estimates than those relying on surface displacement, as also observed for the 2016 Norcia earthquake (Brozzetti et al., 2019), where the displacement measurement was highly variable and affected by local site conditions. The inherited variability in surface expression, combined with the poor preservation potential of coseismic features in unconsolidated deposits, complicates both the recognition and correlation of paleoseismic events across different sites. To account for this uncertainty, we adopted two end-member scenarios for each event: the worst scenario, assuming rupture of the entire fault, and a more conservative alternative constrained by the observed distance between sites where the same event was recognized and sampled.

The variability among different versions of our model assuming different scaling laws (see Figure 4) underscores the importance of rigorously assessing uncertainties in paleoseismic magnitude

estimation, particularly when these data are used to inform seismic hazard assessment. Given their inherent constraints, we emphasize that reliable magnitude estimates using paleoseismic investigations would require extensive fault trenching and multiple measurements to reduce uncertainty to a meaningful range (i.e., at least ± 0.5-1.0 magnitude units). Accordingly, we advocate for the use of at least a 2σ confidence interval when interpreting our magnitude estimates.

Additionally, the completeness of our dataset, although difficult to estimate rigorously, approximately equal to Mw 6.4 implies that smaller paleoevents (Mw 6+) are likely strongly underrepresented. Specifically, we identify it as the sharp detection transition highlighted using the exceedance probability associated with the product of all the probability density functions (**Figure 8**). This limitation restricts the utility of paleoseismology for seismic hazard analysis at least in the context of the central Apennines, Italy, as the mere identification of a paleoearthquake provides little more information than confirming the occurrence of surface-rupturing events in the region. Ultimately, precise magnitude estimation remains a significant challenge, particularly when all relevant sources of uncertainty are properly accounted for - as they must be in any rigorous assessment.

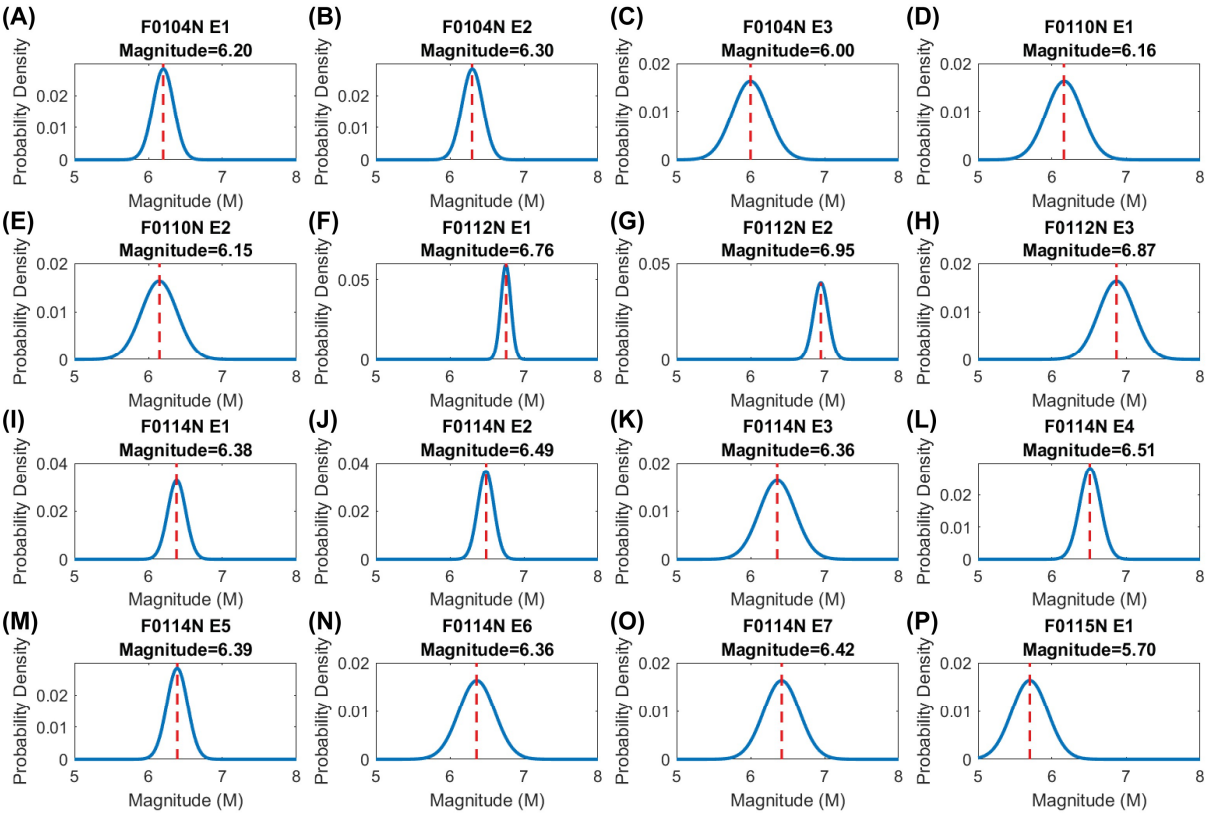

Figure 5: Probability density functions of 16 paleoearthquakes belonging to the PaleoECA_2025 database. They are estimated assuming the magnitudes of large earthquakes follow the Gutenberg-Richter law with b-value = 1.0 and the scaling laws for rupture lengths and throws retrieved by Thingbaijam et al. (2017).

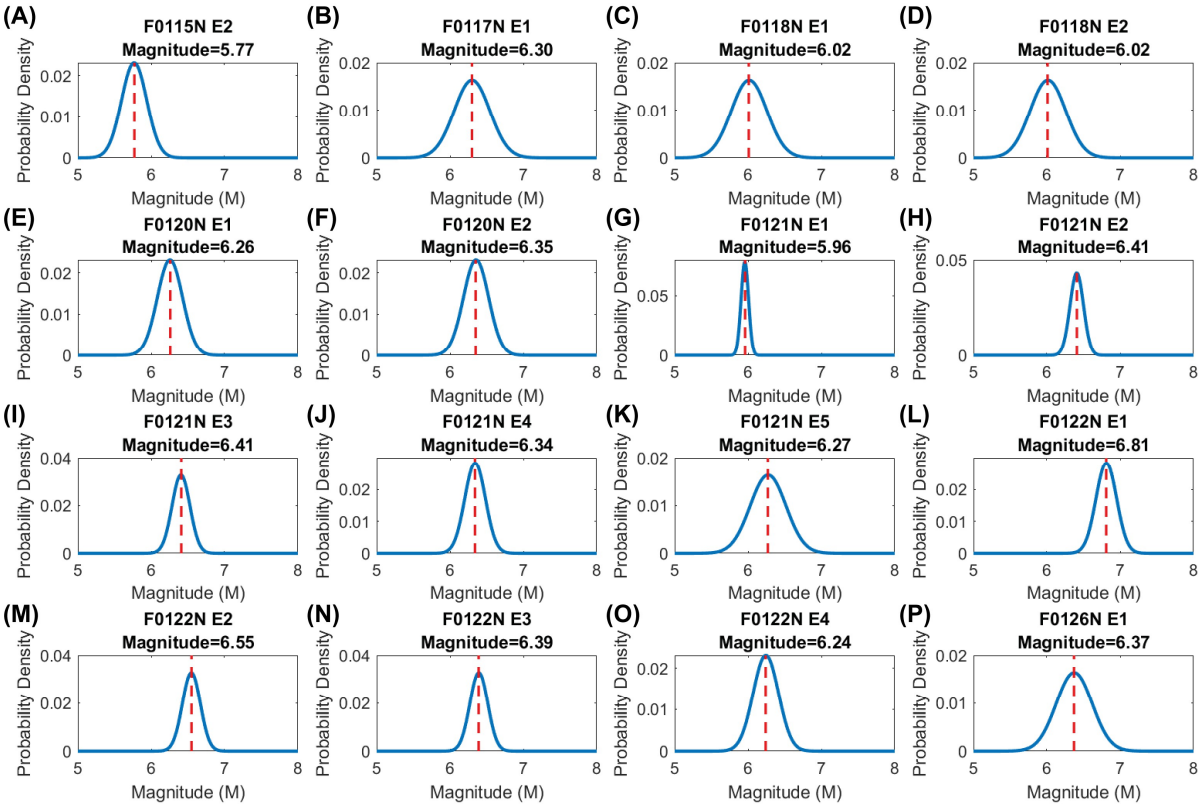

Figure 6: Probability density functions of 16 paleoearthquakes belonging to the PaleoECA_2025 database. They are estimated assuming the magnitudes of large earthquakes follow the Gutenberg-Richter law with b-value = 1.0 and the scaling laws for rupture lengths and throws retrieved by Thingbaijam et al. (2017).

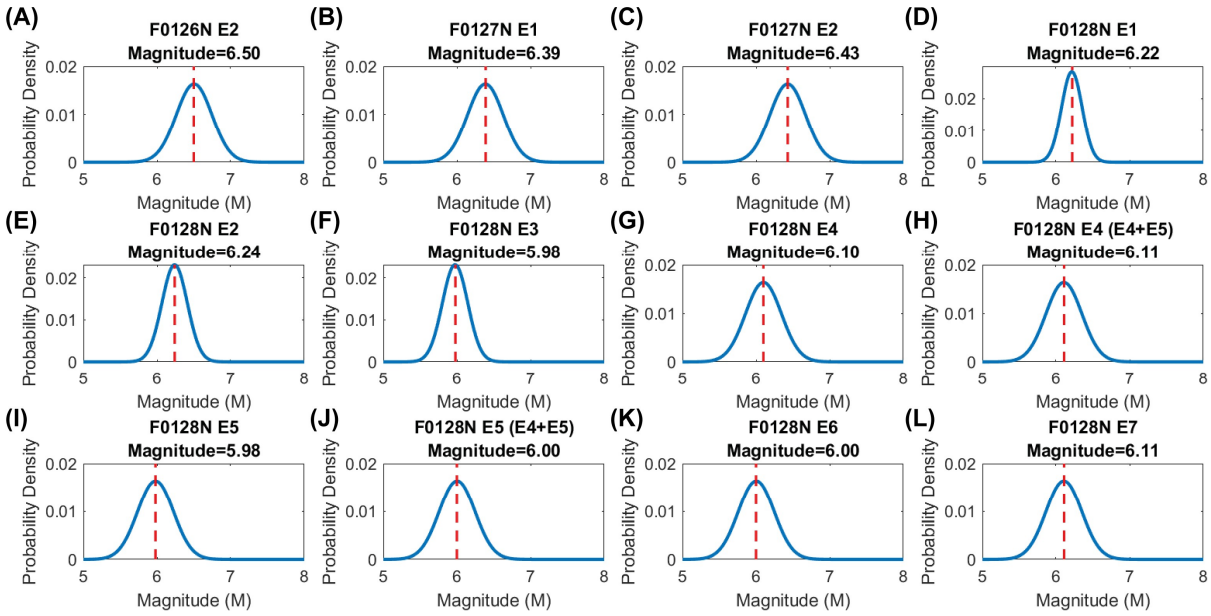

Figure 7: Probability density functions of 12 paleoearthquakes belonging to the PaleoECA_2025 database. They are estimated assuming the magnitudes of large earthquakes follow the Gutenberg-Richter law with b-value = 1.0 and the scaling laws for rupture lengths and throws retrieved by Thingbaijam et al. (2017).

Table 1: List of paleoearthquakes with fault code according to Di Naccio et al. (2025) in column one (see Figure 1 for correspondence). The number of earthquakes (E) are listed in increasing time; the mean value of the Bayesian probability density function and its uncertainty expressed as 2σ are reported in the second and third columns.

Fault Code	Mw	2σ
F0104N E1	6.20	0.28
F0104N E2	6.30	0.28
F0104N E3	6.00	0.48
F0110N E1	6.16	0.48
F0110N E2	6.15	0.48
F0112N E1	6.76	0.14
F0112N E2	6.95	0.20
F0112N E3	6.87	0.48
F0114N E1	6.38	0.24
F0114N E2	6.49	0.22
F0114N E3	6.36	0.48
F0114N E4	6.51	0.28
F0114N E5	6.39	0.28
F0114N E6	6.36	0.48
F0114N E7	6.42	0.48
F0115N E1	5.70	0.48
F0115N E2	5.77	0.34
F0117N E1	6.30	0.48
F0118N E1	6.02	0.48
F0118N E2	6.02	0.48
F0120N E1	6.26	0.34
F0120N E2	6.35	0.34
F0121N E1	5.96	0.10
F0121N E2	6.41	0.18
F0121N E3	6.41	0.24
F0121N E4	6.34	0.28
F0121N E5	6.27	0.48

F0122N E1	6.81	0.28
F0122N E2	6.55	0.24
F0122N E3	6.39	0.24
F0122N E4	6.24	0.34
F0126N E1	6.37	0.48
F0126N E2	6.50	0.48
F0127N E1	6.39	0.48
F0127N E2	6.43	0.48
F0128N E1	6.22	0.28
F0128N E2	6.24	0.34
F0128N E3	5.98	0.34
F0128N E4	6.10	0.48
F0128N E4 (E4+E5)	6.11	0.48
F0128N E5	5.98	0.48
F0128N E5 (E4+E5)	6.00	0.48
F0128N E6	6.00	0.48
F0128N E7	6.11	0.48

361

362

363

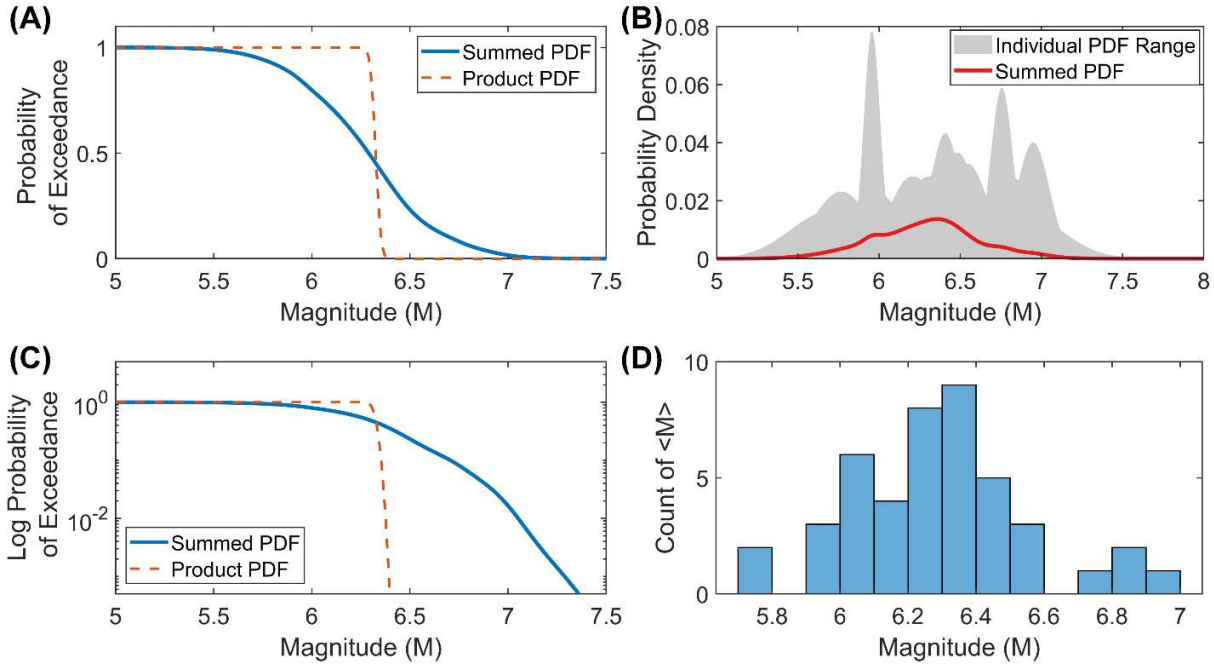

Figure 8: Frequency-size distribution of paleomagnitudes in the PaleoECA_2025 database. (A) Survivor function of the summed (blue line) and multiplied (brown dashed line) probability density distributions of the magnitudes of paleoearthquakes. The product PDF highlights the sharp detection threshold of the catalog close to magnitude Mw 6.4. It suggests that most of the occurred paleoseismic events during the last 25k years below magnitude Mw 6.5 are missing in our database. (B) Individual (shaded gray) and summed (red line) PDFs of the seismic events in PaleoECA_2025. (C) The same exceedance probability in semi-log scale highlighting a line with negative slope above magnitude Mw 6.4 corresponding to the right tail of the Gutenberg-Richter law. (D) Histogram of the mean values of the magnitude PDFs in the PaleoECA_2025 database.

Conclusions

In this study, we present a Bayesian probabilistic framework to estimate the probability density functions (PDFs) of paleomagnitudes through the joint inversion of coseismic surface rupture lengths (L), slip (S), age (T) and associated uncertainties. Our approach is the first to systematically

integrate these parameters into a unified magnitude estimation scheme, leveraging a newly compiled database of 44 paleoseismic events from the central Apennines, Italy (PaleoECA_2025). Our approach is inspired to the works by Biasi and Weldon (2006) and Styron and Sherrod (2021) which we extend including the joint Bayesian inversion of the throws, rupture lengths and time elapsed since the occurrence of the paleoearthquake. We also introduce a more likely prior distribution of magnitudes (the Gutenberg-Richter law instead of a uniform probability), a rigorous testing procedure of the best combination of the scaling laws for accurate magnitude assessment and a precise normalization of posterior probabilities. As a further element of novelty and to facilitate reproducibility and fostering future research, we also release PaleoBAYES, an open-source MATLab software implementing our Bayesian methodology.

A key innovation of our work is the explicit treatment of epistemic and measurement uncertainties inherent in paleoseismological data, which are often overlooked in deterministic scaling relationships. By adopting a probabilistic framework, we account for observational errors in the field, incomplete preservation of surface ruptures, and variability in slip distributions, providing more robust magnitude estimates than traditional regression-based methods. Our results reveal discrepancies with some historical earthquake magnitudes, highlighting the importance of uncertainty-aware approaches in paleoseismology. For instance, the 1915 Fucino earthquake is estimated at Mw 6.76 ± 0.07, lower than classical seismological estimates (Mw > 6.8, Valensise and Pantosti, 2001; Rovida et al., 2020; 2022), but perfectly consistent with other studies (e.g., Gasperini et al., 1999; Paolucci et al., 2016). These findings highlight the need for caution when inferring paleoearthquake magnitudes for seismic hazard assessments, as systematic biases can significantly affect recurrence interval calculations.

For future works we will deal with the dominant issue of scaling laws calibration: current scaling relationships are often derived from global or regional datasets, which may not fully capture local tectonic behavior. New efforts should focus on expanding the Italian paleoseismic database to refine empirical correlations between rupture length, slip, and magnitude. Also, the elapsed time since a paleoearthquake influences the preservation of surface evidence in a much more complex way than modeled in our framework. Our Bayesian approach could be extended to incorporate erosion and sedimentation rates, further reducing systematic biases. Finally, probabilistic paleoseismic magnitude estimates, as demonstrated here through their variability, should be integrated into fault-specific hazard models, particularly in regions with sparse instrumental seismicity.

This study advocates for progressive transition towards a more reliable assessment of paleomagnitudes - from deterministic interpretations to quantitative, uncertainty-quantified - especially when applied to seismic hazard analysis. With PaleoECA_2025 and PaleoBAYES, we respectively provide a new systematic investigation of paleoseismic events in the central Apennines and a shared toolbox hopefully contributing to future community-driven improvements in paleoseismic magnitude estimation.

Conflict of interest statement

Authors declare no conflict of interest.

Data and Resources

The dataset PaleoECA_2025 providing a comprehensive multiparametric paleoseismic database for the central Apennines in Italy will be publicly available on Zenodo upon acceptance of the manuscript. The code PaleoBAYES will be also available at the same link. Throws in Figure 3

for the Amatrice, Norcia and Paganica earthquakes are from Brozzetti et al. (2019) and Nurminen et al. (2022) – listed in the references.

Acknowledgments

The study has been partially funded by the call PRIN2022PNRR, code P2022P37SN—project 'RELATION BETWEEN 3D THERMO-RHEOLOGICAL MODEL AND SEISMIC HAZARD FOR THE RISK MITIGATION IN THE URBAN AREAS OF SOUTHERN ITALY (TRHAM)', Decree of Admission to funding - Director decree no. 1388 of 01/09/2023, ERC sector PE10 'EARTH SYSTEM SCIENCE, FUNDED BY THE EUROPEAN UNION—NEXT GENERATION EU' and by the Istituto Nazionale di Geofisica e Vulcanologia "Progetto Centro Italia DL50 – OR-PER (PEACE)

References

Biasi, G. P., and R. J. Weldon (2006). Estimating surface rupture length and magnitude of paleoearthquakes from point measurements of rupture displacement, *Bull. Seism. Soc. Am.* 96, 1612–1623.

Bird, P. (2007). Uncertainties in long-term geologic offset rates of faults: General principles illustrated with data from California and other western states, *Geosphere* 3, 577–595.

Boncio, P., Pizzi, A., Brozzetti, F., Pomposo, G., Lavecchia, G., Di Naccio, D., and Ferrarini, F. (2010). Coseismic ground deformation of the 6 April 2009 L'Aquila earthquake (central Italy, Mw 6.3). *Geophys. Res. Lett.*, 37(6).

Brozzetti, F., P. Boncio, D. Cirillo, F. Ferrarini, R. De Nardis, A. Testa, and G. Lavecchia (2019). High-resolution field mapping and analysis of the August–October 2016 coseismic surface faulting (central Italy earthquakes): Slip distribution, parameterization, and comparison with global earthquakes, *Tectonics* 38, 417–439.

Carafa, M. M. C., and S. Barba (2013). The stress field in Europe: optimal orientations with confidence limits, *Geophys. J. Int.* 193, 531–548.

Carafa, M. M. C., and P. Bird (2016). Improving deformation models by discounting transient signals in geodetic data: 2. Geodetic data, stress directions, and long-term strain rates in Italy, *J. Geophys. Res. Solid Earth* 121, 5557–5575.

453 Carafa, M. M. C., D. Di Naccio, C. Di Lorenzo, V. Kastelic, and P. Bird (2022). A Meta-
454 Analysis of Fault Slip Rates Across the Central Apennines, *J. Geophys. Res. Solid Earth* 127,
455 e2021JB023252.

456 Carminati, E., and C. Doglioni (2012). Alps vs. Apennines: The paradigm of a tectonically
457 asymmetric Earth, *Earth-Sci. Rev.* 112, 67–96.

458 Chiarabba, C., L. Jovane, and R. DiStefano (2005). A new view of Italian seismicity using 20
459 years of instrumental recordings, *Tectonophysics* 395, 251–268.

460 Cinti, F. R., D. Pantosti, A. M. Lombardi, and R. Civico (2021). Modeling of earthquake
461 chronology from paleoseismic data: Insights for regional earthquake recurrence and earthquake
462 storms in the Central Apennines, *Tectonophysics* 816, 229016.

463 Devoti, R., N. d'Agostino, E. Serpelloni, G. Pietrantonio, F. Riguzzi, A. Avallone, and M.
464 Anzidei (2017). A combined velocity field of the Mediterranean region, *Ann. Geophys.* 60,
465 S0219.

466 Di Domenica, A., A. Turtù, S. Satolli, and F. Calamita (2012). Relationships between thrusts and
467 normal faults in curved belts: new insight in the inversion tectonics of the Central-Northern
468 Apennines (Italy), *J. Struct. Geol.* 42, 104–117.

469 Di Naccio, D., V. Kastelic, M. M. C. Carafa, C. Esposito, P. Milillo, and C. Di Lorenzo (2019).
470 Gravity versus tectonics: The case of 2016 Amatrice and Norcia (central Italy) earthquakes
471 surface coseismic fractures, *J. Geophys. Res. Earth Surf.* 124, 994–1017.

472 DuRoss, C. B., S. F. Personius, A. J. Crone, S. S. Olig, and W. R. Lund (2011). Integration of
473 paleoseismic data from multiple sites to develop an objective earthquake chronology:
474 Application to the Weber segment of the Wasatch fault zone, Utah, *Bull. Seism. Soc. Am.* 101,
475 2765–2781.

476 EMERGEO Working Group. (2010). Evidence for surface rupture associated with the Mw 6.3
477 L'Aquila earthquake sequence of April 2009 (central Italy). *Terra Nova*, 22(1), 43-51.

478 Faure Walker, J., P. Boncio, B. Pace, G. Roberts, L. Benedetti, O. Scotti, and L. Peruzza (2021).
479 Fault2SHA Central Apennines database and structuring active fault data for seismic hazard
480 assessment, *Sci. Data* 8, 87.

481 Frepoli, A., G. B. Cimini, P. De Gori, G. De Luca, A. Marchetti, S. Monna, and N. M. Pagliuca
482 (2017). Seismic sequences and swarms in the Latium-Abruzzo-Molise Apennines (central Italy):
483 New observations and analysis from a dense monitoring of the recent activity, *Tectonophysics*
484 712, 312–329.

485 Galadini, F., and P. Galli (2000). Active tectonics in the central Apennines (Italy)–input data for
486 seismic hazard assessment, *Nat. Hazards* 22, 225–268.

Galli, P. (2020). Recurrence times of central-southern Apennine faults (Italy): hints from palaeoseismology, *Terra Nova* 32, 399–407.

Galli, P. A., B. Giaccio, P. Messina, E. Peronace, and G. M. Zuppi (2011). Palaeoseismology of the L'Aquila faults (central Italy, 2009, M w 6.3 earthquake): Implications for active fault linkage, *Geophys. J. Int.* 187, 1119–1134.

Gasperini, P., Bernardini, F., Valensise, G., and Boschi, E. (1999). Defining seismogenic sources from historical earthquake felt reports. *Bull. Seismol. Soc. Am.* 89(1), 94-110.

Gómez-Novell, O., B. Pace, F. Visini, J. Faure Walker, and O. Scotti (2023). Deciphering past earthquakes from the probabilistic modeling of paleoseismic records–the Paleoseismic EArthquake CHronologies code (PEACH, version 1), *Geosci. Model Dev.* 16, 7339–7355.

ISIDe Working Group (2007). Italian Seismological Instrumental and Parametric Database (ISIDe), Istituto Nazionale di Geofisica e Vulcanologia (INGV), https://doi.org/10.13127/ISIDE.

Kastelic, V., P. Burrato, M. M. Carafa, and R. Basili (2017). Repeated surveys reveal nontectonic exposure of supposedly active normal faults in the central Apennines, Italy, *J. Geophys. Res. Earth Surf.* 122, 114–129.

Latorre, D., R. Di Stefano, B. Castello, M. Michele, and L. Chiaraluce (2023). An updated view of the Italian seismicity from probabilistic location in 3D velocity models: The 1981–2018 Italian catalog of absolute earthquake locations (CLASS), *Tectonophysics* 846, 229664.

Lavecchia, G., F. Brozzetti, M. Barchi, M. Menichetti, and J. V. Keller (1994). Seismotectonic zoning in east-central Italy deduced from an analysis of the Neogene to present deformations and related stress fields, *Geol. Soc. Am. Bull.* 106, 1107–1120.

Lavecchia, G., S. Bello, C. Andrenacci, D. Cirillo, F. Ferrarini, N. Vicentini, and F. Brozzetti (2022). QUaternary fault strain INdicators database-QUIN 1.0-first release from the Apennines of central Italy, *Sci. Data* 9, 204.

Leonard, M. (2010). Earthquake fault scaling: Self-consistent relating of rupture length, width, average displacement, and moment release, *Bull. Seism. Soc. Am.* 100, 1971–1988.

Leonard, M. (2014). Self-consistent earthquake fault-scaling relations: Update and extension to stable continental strike-slip faults, *Bull. Seism. Soc. Am.* 104, 2953–2965.

Lombardi, A. M., Cinti, F. R., and Pantosti, D. (2025). Paleoearthquakes modelling and effects of uncertainties on probability assessment of next fault ruptures: the case of Central Italy surface faulting earthquakes. *Geophys. J. Intern.*, 241(2), 1327-1347. https://doi.org/10.1093/gji/ggaf105

Mariucci, M. T., and P. Montone (2025). IPSI 1.7, Database of Italian Present-day Stress Indicators, Istituto Nazionale di Geofisica e Vulcanologia (INGV), https://doi.org/10.13127/IPSI.1.7.

Montone, P., and M. T. Mariucci (2016). The new release of the Italian contemporary stress map, *Geophys. J. Int.* 205, 1525–1531.

Nurminen, F., Baize, S., Boncio, P., Blumetti, A. M., Cinti, F. R., Civico, R., and Guerrieri, L. (2022). SURE 2.0–New release of the worldwide database of surface ruptures for fault displacement hazard analyses. *Sci. Data*, 9(1), 729.

Paolucci, R., Evangelista, L., Mazzieri, I., and Schiappapietra, E. (2016). The 3D numerical simulation of near-source ground motion during the Marsica earthquake, central Italy, 100 years later. *Soil Dynam. Earthq. Eng.*, 91, 39-52.

Patacca, E., P. Scandone, E. Di Luzio, G. P. Cavinato, and M. Parotto (2008). Structural architecture of the central Apennines: Interpretation of the CROP 11 seismic profile from the Adriatic coast to the orographic divide, *Tectonics* 27, TC3007.

Pavlides, S., and R. Caputo (2004). Magnitude versus faults' surface parameters: quantitative relationships from the Aegean Region, *Tectonophysics* 380, 159–188.

Pizzi, A., and F. Galadini (2009). Pre-existing cross-structures and active fault segmentation in the northern-central Apennines (Italy), *Tectonophysics* 476, 304–319.

Pondrelli, S., and A. Morelli (2008). Seismic strain and stress field studies in Italy before and after the Umbria–Marche seismic sequence: a review, *Ann. Geophys.* 51, 3–17.

Pondrelli, S., and S. Salimbeni (2006). Italian CMT dataset, https://doi.org/10.13127/ISIDE.

Porreca, M., A. Fabbrizzi, S. Azzaro, S. Pucci, L. Del Rio, P. P. Pierantoni, and M. R. Barchi (2020). 3D geological reconstruction of the M. Vettore seismogenic fault system (Central Apennines, Italy): Cross-cutting relationship with the M. Sibillini thrust, *J. Struct. Geol.* 131, 103938.

Ramsey, C. B. (2009). Bayesian analysis of radiocarbon dates, *Radiocarbon* 51, 337–360.

Rovida, A., Locati, M., Camassi, R., Lolli, B., and Gasperini, P. (2020). The Italian earthquake catalogue CPTI15. *Bull. Earth. Eng.* 18, 2953-2984.

Rovida, A., M. Locati, R. Camassi, B. Lolli, P. Gasperini, and A. Antonucci (2022). Catalogo parametrico dei terremoti italiani (cpti15). INGV versione 4.0, https://doi.org/10.13127/CPTI/CPTI15.4.

Serva, L. (1986). Gli effetti sul terreno del terremoto del Fucino (13-1-1915); tentativo di interpretazione della evoluzione tettonica recente di alcune strutture, in Geologia dell'Italia centrale. Congresso nazionale. 73, 387–390.

552 Styron, R. H., and B. Sherrod (2021). Improving paleoseismic earthquake magnitude estimates
553 with rupture length information: Application to the Puget Lowland, Washington State, USA,
554 *Bull. Seism. Soc. Am. 111*, 1139–1153.

555 Thingbaijam, K. K. S., P. M. Mai, and K. Goda (2017). New empirical earthquake source-scaling
556 laws, *Bull. Seism. Soc. Am.* 107, 2225–2246.

557 Valensise, G., and Pantosti, D. (2001). The investigation of potential earthquake sources in
558 peninsular Italy: a review. *J. Seismol.*, 5(3), 287-306.

559 Valoroso, L., L. Chiaraluce, D. Piccinini, R. Di Stefano, D. Schaff, and F. Waldhauser (2013).
560 Radiography of a normal fault system by 64,000 high-precision earthquake locations: The 2009
561 L'Aquila (central Italy) case study, *J. Geophys. Res. Solid Earth* 118, 1156–1176.

562 Walters, R. J., Elliott, J. R., D'agostino, N., England, P. C., Hunstad, I., Jackson, J. A., ... and
563 Roberts, G. (2009). The 2009 L'Aquila earthquake (central Italy): A source mechanism and
564 implications for seismic hazard. *Geophys. Res. Lett.*, 36(17).

565 Wells, D. L., and K. J. Coppersmith (1994). New empirical relationships among magnitude,
566 rupture length, rupture width, rupture area, and surface displacement, *Bull. Seism. Soc. Am.* 84,
567 974–1002.